Energetics and electronic structure of point defects associated with oxygen excess at a tilt boundary of ZnO

Fumiyasu Oba[a] and Hirohiko Adachi
Department of Materials Science and Engineering, Kyoto University, Sakyo, Kyoto 606-8501, Japan
Isao Tanaka
Department of Energy Science and Technology, Kyoto University, Sakyo, Kyoto 606-8501, Japan

(Received 3 May 2000; accepted 20 July 2000)

The formation energies and electronic structure of zinc vacancies and oxygen interstitials at a tilt boundary of ZnO were investigated by a combination of static lattice and first-principles molecular orbital methods. For both of the defect species, the formation energies were lower than those of the bulk defects at certain sites in the grain boundary. The defects with low formation energies formed electronic states close to the top of the valence band. The interfacial electronic states observed experimentally in ZnO varistors cannot be explained solely by the point defects associated with the oxygen excess: the effects of impurities should be significant for the states.

I. INTRODUCTION

It is well known that mechanical and electrical properties of polycrystalline ceramics often originate from their grain boundaries. One of the most interesting phenomena is the nonlinear current–voltage characteristics exhibited in ZnO ceramics with additives such as Bi_2O_3, Pr_6O_{11}, and 3d transition-metal oxides.[1–3] The characteristics are widely utilized as varistors to protect electric circuits against overvoltage. The appearance of the nonlinear characteristics has been ascribed to the formation of the double Schottky barriers at the grain boundaries.[4,5] The barrier is generated by the charge transfer from donor-type bulk states to acceptor-type interface states in order to equilibrate the Fermi level. Theoretical calculations of the current–voltage characteristics of ZnO ceramics have been carried out on the basis of the double Schottky barrier model, and the results are consistent with observed characteristics.[4,6,7] According to them, the nonlinear behavior is determined mainly by the shape, energy, and charge of the interface states. The interface states have also been investigated experimentally and detected to form 0.6–1.0 eV below the bottom of the conduction band.[8–13] However, the explicit origin of the interface states is still unknown. As the candidates of the origin, atomic arrangements and the segregation of point defects at the grain boundaries can be suggested. Disturbed atomic arrangements at the grain boundaries may generate specific electronic states. We have previously investigated the electronic structure of the [0001]/($\bar{1}$230) Σ7 symmetric tilt boundary in ZnO by a combination of static lattice and first-principles molecular orbital methods.[14] Some types of equilibrium geometric configurations with and without dangling bonds are obtained with similar boundary energies. However, deep interfacial electronic states are not recognized within the band gap even in the configurations with dangling bonds. First-principles calculations for the coincident site lattice (CSL)[15] tilt boundaries in Al_2O_3 and TiO_2 have also been performed by Mo *et al.*[16] and Dawson *et al.*,[17] respectively. In their results, deep interface states are not recognized, either. Although these are reports on the special boundaries, the generation of deep interface states in ZnO varistors may not be explained solely by atomic arrangements at stoichiometric boundaries.

Intrinsic defects and impurities naturally form specific electronic states, and therefore, the segregation of the point defects at the grain boundary should correspond to the formation of interfacial electronic states. Regarding the intrinsic defects, excessive oxygen at the grain boundary has been suggested as the origin of the interface states.[9,18,19] This is consistent with experimental reports in which varistor characteristics depend largely on oxygen partial pressure during heat treatment and sintering processes.[10,20,21] Hayashi *et al.* reported that the density of interface states increases with the oxygen partial pressure, using deep-level transient spectroscopy (DLTS).[10] Stucki *et al.* observed that oxygen accumulation is more abundant at the intergranular-fractured surface in the untreated sample than in the electrically degraded sample by the x-ray photoelectron spectroscopy.[22,23] Because ZnO exhibits *n*-type conductivity due to the presence of donor-type intrinsic defects such as

[a]Address all correspondence to this author.
e-mail oba@dvxa4.mtl.kyoto-u.ac.jp

zinc interstitials and oxygen vacancies,[24–27] oxygen should be slightly poor in the bulk region. The excess of oxygen at the boundary region may be considered as the compensation of the donor-type defects and/or the segregation of acceptor-type defects such as zinc vacancies and oxygen interstitials.

As for the impurities, the contribution of 3d transition-metal ions to the interface states has been suggested by Yano *et al.*, on the basis of the investigation of the fabricated ZnO/$PrCoO_x$/ZnO junctions containing Mn, Co, or Cu impurities by DLTS.[28,29] The role of 3d transition-metal impurities to stabilize oxygen adsorption has also been suggested.[30–32] This is consistent with the fact that doping of the impurities is necessary to obtain the nonlinear characteristics.

Thus both of the excessive oxygen and the impurities are likely to contribute to the interfacial electronic states. In this paper, we focus only on the electronic states induced by the excessive oxygen. Although the excess of oxygen is presumably related to the presence of the impurities according to the above reports, it should be significant to investigate the electronic states associated with the excessive oxygen itself, discriminating from the effects of the impurities. The excessive oxygen is assumed to be zinc vacancies or oxygen interstitials, and the electronic states induced by the point defects at a symmetric tilt boundary of ZnO, the [0001]/$(\bar{1}\bar{2}30)$ $\Sigma 7$, are investigated. The atomic and electronic structures of CSL boundaries in metal oxides such as MgO, NiO, Al_2O_3 TiO_2, and ZnO have been discussed both experimentally[33–36] and theoretically.[14,16,17,37–43] Although the CSL boundaries are not necessarily representative of boundaries in polycrystalline ceramics, it facilitates understanding the correlation between the atomic structures and the properties.

The procedure of this study is as follows. First we perform static lattice calculations for zinc vacancies and oxygen interstitials to obtain the equilibrium atomic arrangements and formation energies. The electronic structures of the derived atomic arrangements are then calculated by a first-principles molecular orbital method. Electronic states and chemical bonding specific to the point defects at the grain boundary are discussed in comparison with those in the bulk.

II. STATIC LATTICE CALCULATION

A. Methodology

Static lattice calculations were performed employing the computer code GULP.[44] The total internal energies of simulation cells were iteratively minimized under 3-dimensional periodic boundary conditions using quasi-Newton method with Broyden–Fletcher–Goldfarb–Shanno hessian update scheme.[45] The lattice energy was decomposed into a long-range electrostatic energy and a short-range repulsive energy. The electrostatic energy was calculated using the Ewald summation scheme assuming the formal ionic charges of ±2. Two-body potentials of the Buckingham form were used to model short-range repulsive interactions; i.e.,

$$V_{ij}(r_{ij}) = A_{ij}\exp(-r_{ij}/\rho_{ij}) - C_{ij}/r_{ij}^6 \quad . \qquad (1)$$

Potential parameters reported by Lewis *et al.* were used, which are listed in Table I. The cut-off distances of the Buckingham potentials were set to be 6 and 12 Å for Zn^{2+} – O^{2-} and O^{2-}–O^{2-}, respectively. For oxygen ions, core–shell polarization was considered by the Harmonic spring with the force constant K. The bulk properties of wurtzite ZnO are reproduced satisfactorily using the potentials, as listed in Table II. The errors of the lattice constants, +0.5% for a, −2.6% for c, and +2.5% for u, have previously been confirmed not to influence electronic structure significantly.[14]

The calculations of defect formation energies and atomic arrangements around the defects are performed on the basis of the Mott–Littleton method.[50,51] The crystal around the defect is divided into three spherical regions, i.e., regions 1, 2a, and 2b. Ions in the region 1 are allowed to relax explicitly. In the region 2a, the displacement of ions is considered under the assumption that the ions are in a harmonic well, whereas only the implicit polarization of sublattices results from a defect charge is considered in the region 2b. In the present calculations, the sizes were chosen to be 10 and 20 Å for regions I and 2a, respectively.

For the calculations of zinc vacancies and oxygen interstitials, the charge state of 2– was assumed. In ZnO varistors, grains exhibit n-type conductivity with the donor concentrations in the order of 10^{16} to 10^{18} cm^{-3}.[9,13,52] The donor energies have been reported to be 0.05–0.2 eV, and the Fermi levels have been estimated to be very close to the bottom of the conduction band. The acceptor-type defects dealt with in the present study are expected to have the highest charge states of 2– with such high Fermi levels.[53–55] Under the assumption, all of the zinc and oxygen ions approximately have the formal charge of ±2, and therefore the above potentials were applied to the defect calculations without any modification. We have tested the potentials thoroughly with

TABLE I. Parameters for two-body potentials.

Buckingham	A(eV)	ρ (Å)	C (eV Å^6)
Zn^{2+}–O^{2-}	700.3	0.3372	0
O^{2-}–O^{2-}	22764	0.149	27.879
		Charge	
Harmonic spring	K(eV Å^{-2})	O^{2-}(core)	O^{2-}(shell)
O^{2-}(core)–O^{2-}(shell)	74.92	0.86902	−2.86902

TABLE II. Calculated bulk properties of wurtzite ZnO.

		This work	Literature
Lattice constants	a (Å)	3.2677	3.2507 (Exp.)[a]
	c (Å)	5.0741	5.2083
	u	0.3920	0.3825
Mean interatomic distance (Å)	Zn–O	1.9707	1.9786
	Zn–Zn(O–O)	3.2147	3.2303
Elastic constants (GPa)	c_{11}	236	210 (Exp.)[b]
	c_{12}	116	121
	c_{13}	105	105
	c_{33}	188	211
	c_{44}	74	43
Bulk modulus (GPa)		145	144 (Exp.)[b]
			160 (Calc.)[c]
			(183 (Exp.)

[a]Ref. 47.
[b]Ref. 48.
[c]Ref. 49.

the aid of a first-principles plane-wave pseudopotential method for the bulk defects. The first-principles calculations were performed for the super cells containing 72 atoms and a defect using the CASTEP code.[56] The positions of the first nearest neighbors of the defects are compared under the condition that the first and the second nearest neighbors of the defects are allowed to relax. The mean differences of atomic positions in between the results of the present static lattice calculations and those by the first-principles calculations are less than 0.1 Å. The tendency that the vacancy exhibits the lowest formation energy and the interstitial at the octahedral site does the second is common to both results. We believe that the accuracy is good enough to discuss the atomic arrangements and relative energetics of the defects.

The formation energies of the defects were calculated as

$$E_{\text{formation}} = E_{\text{defective}} - n_{\text{Zn}}\mu_{\text{Zn}} - n_{\text{O}}\mu_{\text{O}} \quad , \\ = E_{\text{defective}} - (n_{\text{O}} - 1)\mu_{\text{ZnO}} - \mu_{\text{O}} \quad , \qquad (2)$$

where $E_{\text{defective}}$ is the total energy of a defective configuration containing n_{Zn} Zn atoms and n_{O} O atoms. For the zinc vacancies and the oxygen interstitials, $n_{\text{zn}} - n_{\text{O}} = -1$. μ_{Zn} and μ_{O} are the chemical potentials, and they are correlated as $\mu_{\text{Zn}} + \mu_{\text{O}} = \mu_{\text{ZnO}}$. For the bulk defects, μ_{ZnO} is obtained by the calculation of the ZnO perfect lattice. However, the reference of the perfect lattice may not be valid for the defects at the grain boundary because the grain boundary is not in equilibrium with the bulk: the reference makes the formation energy include the grain boundary energy. It may therefore be good to choose the grain boundary without the defects as the $(n_{\text{O}} - 1)\mu_{\text{ZnO}}$ in Eq. (2). In this case, the formation energy corresponds to the increase in total energy by the presence of defects, as that for the bulk defects is.

The formation energies of the charged defects depend on the electronic chemical potential, in addition to the chemical potential of the oxygen μ_{O}.[53–55,57] In the present study, μ_{O} is chosen to be equal to the half of μ_{ZnO} and the electronic chemical potential is neglected for simplicity. However, the formation energies of the zinc vacancies and the oxygen interstitials can be discussed relatively since the difference of the energies is independent of both of the oxygen and the electronic chemical potentials.

Regarding defect sites at the [0001]/($\bar{1}\bar{2}30$) $\Sigma 7$ symmetric tilt grain boundary of ZnO, the equilibrium boundary geometry calculated in our previous work[14] was employed as initial atomic coordinates. The atomic structure is shown in Fig. 1. This configuration has the boundary energy of 1.37 J m^{-2} (0.086 eV Å^{-2}). Contrary to the sixfold coordinated channels in the [000$\bar{1}$] view of the wurtzite structure, the boundary core structure can be regarded as a sequence of fourfold and eightfold coordinated channels. All the ions have the complete fourfold coordination of ions of opposite sign as in the bulk region although there are ions of like sign at a close distance around the fourfold coordinated channels.

Using a 192-atom supercell containing two identical boundaries, this initial structure was calculated under 3-dimensional periodic boundary conditions. The distance between the boundaries of 26 Å has reduced boundary–boundary interaction sufficiently: the boundary energy has converged within 0.03 J m^{-2} (0.002 eV Å^{-2}) relative to the results with the distance of 41 Å. For the calculation of the zinc vacancies at the boundary, the zinc sites on the columns labeled with capitals in Fig. 1 were considered. The sites labeled with small letters were chosen for the oxygen interstitials. The a site is in the eightfold coordinated channel. The other sites are in the sixfold coordinated channels and have

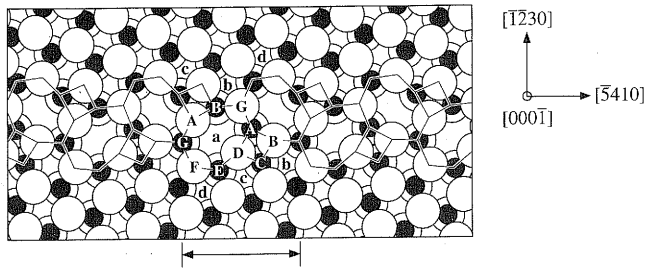

FIG. 1. View of the calculated geometry of the [0001]/($\bar{1}\bar{2}30$) boundary in ZnO from the [000$\bar{1}$] direction. Filled and open circles denote zinc and oxygen ions. The scale indicates a periodicity unit. The boundary core structure is described as a sequence of fourfold and eightfold coordinated channels. Three of the four basal planes in the wurtzite structure can be seen in the order of O–Zn–O. The sites labeled with capitals and small letters are considered for the zinc vacancies and the oxygen interstitials, respectively.

surroundings of the nearest neighbors similar to those of the octahedral interstitial site in the bulk. For comparative discussion, calculations of the defects in the bulk were also performed. In this case, two interstitial sites, i.e., octahedral and tetrahedral sites, were considered for the oxygen interstitials.

B. Results and discussion

Calculated properties of the defects are listed in Table III. The atomic arrangement with the lowest formation energy for each defect species in the bulk or at the grain boundary is also shown in Fig. 2.

For the zinc vacancy in the bulk, outward relaxation of the four oxygen ions adjacent to the vacancy is remarkable in Fig. 2(a). This makes the mean distance between the four oxygen ions and their neighboring zinc ions 6.4% shorter than that of 1.971 Å in the perfect lattice. The oxygen ions are surrounded by the 12 oxygen ions of the second nearest neighbor as those in the perfect lattice although the distances are slightly different due to the relaxation. For the grain boundary, the zinc vacancy at the C site in Fig. 1 exhibits the lowest formation energy. Outward relaxation similar to the bulk vacancy is recognized in Fig. 2(c). In the original geometry before introduction of the vacancy, the zinc ions at the A and the C sites are very close. This unfavorable surrounding may suggest why the vacancy at this site exhibits the lowest formation energy. In practice, the zinc vacancies at the A–D sites, which have such unfavorable surroundings in the original geometries, show lower formation energies than the vacancies at the other sites, E–G. This may also be the reason for the lower formation energy of the vacancies at the A–D sites than the bulk vacancy. At the E–G sites, the formation energies are close to or higher than the bulk vacancy.

For the oxygen interstitial in the bulk, the interstitial at the octahedral site exhibits lower formation energy. At the tetrahedral site, the oxygen interstitial is neighboring four zinc ions with the mean distance of 1.870 Å. The most possible reason for the higher formation energy is the fact that one oxygen ion is present at a distance of 2.106 Å. Although the large relaxation to lengthen the distance has taken place, this is nevertheless too short for the distance between oxygen ions: the mean distance between oxygen ions is 3.215 Å for the perfect lattice. On the other hand, the oxygen interstitial is surrounded by six zinc ions with the mean distance of 2.094 Å at the octahedral site, as shown in Fig. 2(b). Although the distance is slightly larger than that at the perfect lattice sites, this site is also small for the oxygen interstitial. Six oxygen ions are present at the mean distance of 2.542 Å, which is considerably close relative to the original distance between oxygen ions. For the grain boundary, the oxygen interstitial at the a site in Fig. 1 exhibits the lowest formation energy. At the b and the d sites, the formation energies are close to that at the bulk octahedral site presumably due to similar local surroundings. For the c site, the initial surroundings are also similar to the bulk octahedral site: the oxygen interstitial is neighboring to six zinc ions. However, the large relaxation of the ions adjacent to the eightfold channel has taken place to enlarge the interstitial site and the coordination number of 6 has been reduced to 4. The resultant formation energy is lower than those at the b and the d sites, but higher than that at the a site. For the oxygen interstitial at the a site, which shows the lowest formation energy, the oxygen interstitial is surrounded by four zinc ions as shown in Fig. 2(d). The mean O–Zn distance of 2.050 Å is slightly larger than that at the lattice site. There are six oxygen ions at the mean distance of 2.785 Å, and the distances from other oxygen ions are larger than that of the perfect lattice. The surroundings of the neighboring oxygen ions are more preferable than those of the oxygen interstitials at the other sites of the grain boundary and the bulk. This may be the main reason that this configuration shows the lowest formation energy.

In summary, the formation energies of the defects can be lowered at certain sites in the grain boundary. For the zinc vacancies, this can be explained by the release of mismatch strain at the core of the vacancies. Zinc vacancies can more easily form where zinc ions have less favorable surroundings before introduction of the vacancies. On the other hand, the presence of larger interstitial site lowers the formation energy at the present boundary in the case of the oxygen interstitials.

TABLE III. Calculated properties of zinc vacancies and oxygen interstitials in the bulk and at the grain boundary. The mean distance of O–Zn denotes that between oxygen ions adjacent to the vacancy and their neighboring zinc ions for the zinc vacancy, whereas that between the oxygen interstitial and its neighboring zinc ions for the oxygen interstitial. The coordination numbers are shown in the parentheses.

	Defect	Site	Formation energy (eV)	Mean O–Zn distance (Å)
Bulk	V_{Zn}		3.7	1.844(3)
	O_i	Octahedral	4.6	2.094(6)
		Tetrahedral	6.3	1.870(4)
Grain boundary	V_{Zn}	A	2.8	1.857(3)
		B	3.3	1.844(3)
		C	2.4	1.865(3)
		D	3.0	1.861(3)
		E	3.3	1.868(3)
		F	3.6	1.849(3)
		G	4.2	1.853(3)
	O_i	a	3.4	2.050(4)
		b	4.4	2.082(6)
		c	3.7	2.012(4)
		d	4.2	2.101(6)

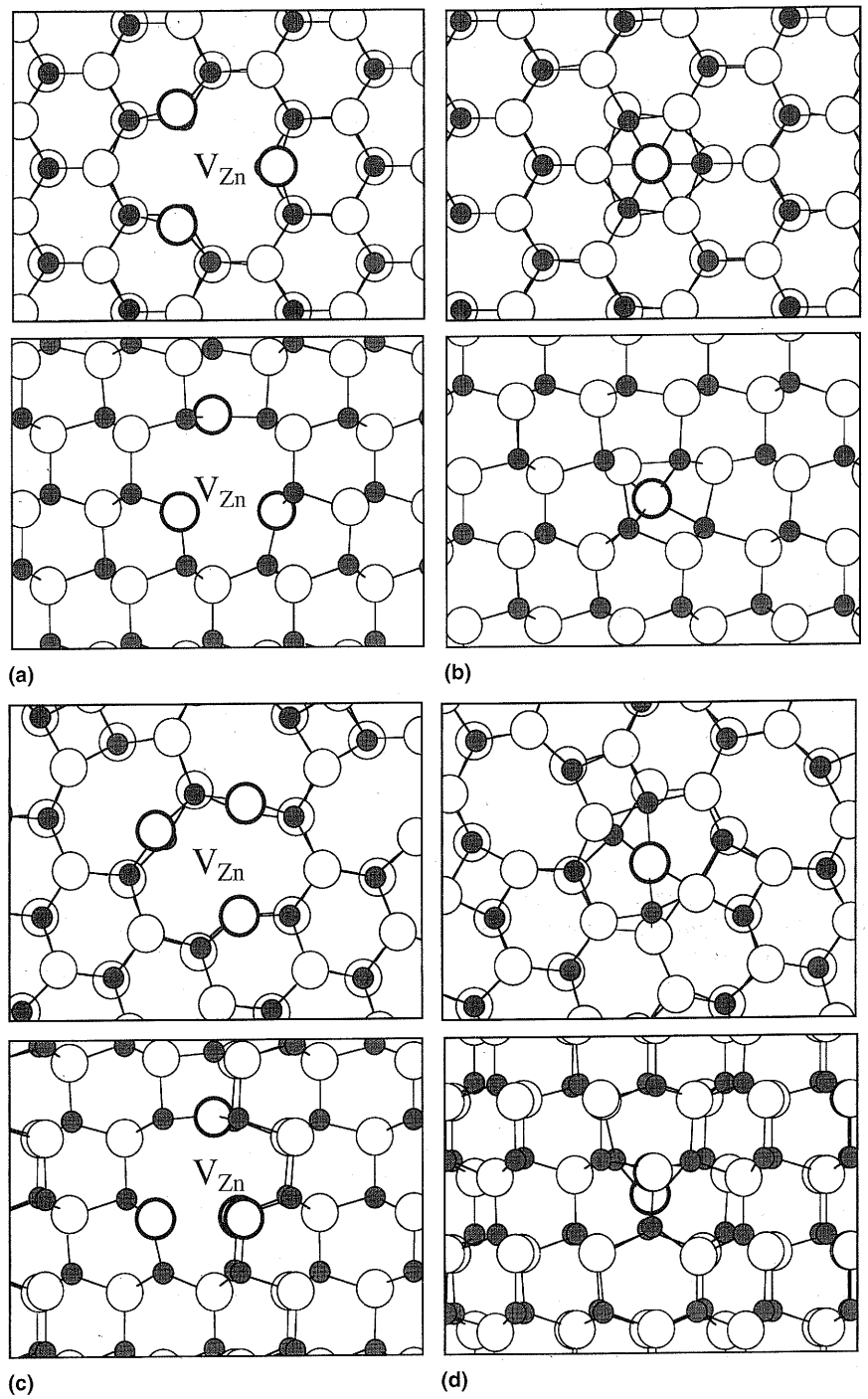

FIG. 2. View of the optimized geometries in the vicinity of the defects: (a) the zinc vacancy, (b) the oxygen interstitial at the octahedral site in the bulk from the [000$\bar{1}$] (upper) and the [2$\bar{1}$ $\bar{1}$0] (lower) directions, (c) the zinc vacancy at the C site, and (d) the oxygen interstitial at the a site of the grain boundary from the [000$\bar{1}$] (upper) and the [$\bar{1}$ $\bar{2}$30] (lower) directions. Filled and open circles denote zinc and oxygen ions. The oxygen ions adjacent to the zinc vacancies or at the interstitial sites are shown with bold circles. Ions at the columns including vacancy sites are not shown for easy recognition of vacancy sites.

III. MOLECULAR ORBITAL CALCULATION

A. Methodology

Electronic structure calculations have been carried out by the discrete variational (DV)–Xα method[58] employing the computer code SCAT.[59] The electronic structures of model clusters are self-consistently obtained by solving one-electron Schrödinger equations within the local density approximation. Molecular orbitals are represented by the linear combination of atomic orbitals. The atomic orbitals are numerically obtained by solving a radial part of a Schrödinger equation for each atom. The

atomic charge density is renewed using atomic orbital populations in molecular orbitals by the Mulliken population analysis[60] at each iteration until it is also self-consistent. In other words, the atomic basis functions are optimized under given chemical environments. Fairly accurate molecular orbital calculations can therefore be done using only a nearly minimal number of basis functions. 1s–2p for oxygen and 1s–4p for zinc are sufficient to reproduce the core and the valence states of ZnO. The use of the nearly minimal basis functions enables the investigation of chemical bonding by the Mulliken population analysis. Net charges and overlap populations, measures of ionicity and covalent bonding strength, respectively, were obtained by the population analysis using the nearly minimal basis functions. In case that the energies of electronic states are discussed quantitatively, Zn–4d and –5sp orbitals were added for a better description of the high energy states near the conduction band.

A model cluster containing 105 to 153 atoms was constructed according to the optimized configuration with the lowest formation energy for each defect species: the zinc vacancy and the oxygen interstitial at the octahedral site for the bulk, and the zinc vacancy at the C site and the oxygen interstitial at the A site for the grain boundary. To investigate the relationship between the formation energy and the electronic structure more systematically, calculations were also performed for two other samples: the oxygen interstitial at the bulk tetrahedral site, which exhibits the highest formation energy among all the defects dealt with in the present study, and the zinc vacancy at the boundary A site, which exhibits the second lowest formation energy. We have confirmed that the one-electron energies of defect levels are converged well with respect to the cluster size for the bulk defects: the differences in the energies are within 0.05 eV in the above range of the cluster size. As an example, Fig. 3 shows the structure of the $[Zn_{36}O_{71}]^{70-}$ model cluster for the grain boundary with the oxygen interstitial at the a site. The clusters were constructed on the basis of a connection of ZnO_4 tetrahedral units to include three Zn- and four O-basal planes. To take electrostatic potential into account and minimize the termination effects of the finite-sized clusters, the clusters were embedded in about 10,000 point charges with the charge of ±2 located at the external atomic sites. For comparative discussion, calculations were also performed for the bulk and the grain boundary without the defects.

B. Results and discussion

The one-electron energy level structure for the configuration with the lowest formation energy for each defect species is shown in Fig. 4. The energy levels were shifted to align the mean energies of O-2s bands because they should reflect the mean electrostatic potentials for

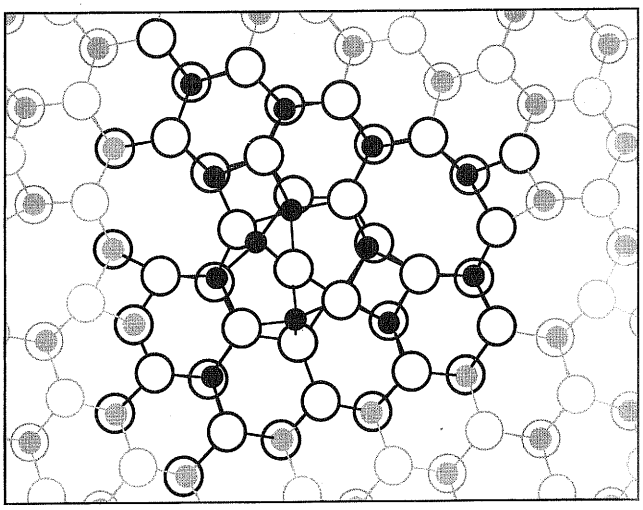

FIG. 3. View of the $[Zn_{36}O_{71}]^{70-}$ model cluster for the grain boundary with an oxygen interstitial from the $[000\bar{1}]$ direction. Filled and open black circles denote zinc and oxygen ions in the cluster. ±2 point charges were put on the sites of gray circles.

respective model cluster. In ZnO, the valence band is mainly composed of Zn-3d and O-2p. The unoccupied conduction band constructed mainly by Zn-4sp and -5sp lies above the band gap. The density of states calculated from the energy levels of the bulk model without the defects is in good agreement with the results of band calculations by Schröer *et al.*[61] and by Xu *et al.*[62] as shown elsewhere.[14] In this model, the gap between the highest occupied level and the lowest unoccupied level is 1.83 eV. This value is smaller than the experimental band gap of 3.30 eV[63] due to the local density approximation.

For the bulk zinc vacancy model, acceptor-type levels which are mainly composed of 2p orbitals of the oxygen ions adjacent to the vacancy form near the top of the valence band. These are occupied because of the assumption of the charge state 2–. In other words, two electrons are trapped on the acceptor-type levels. Similar levels are also created in the case of the bulk oxygen interstitial model. However, the energies of the levels are considerably higher presumably due to the large antibonding interaction with the closely surrounding oxygen ions as discussed later. In the case of the grain boundary model without the defects, the valence band spreads slightly toward both the higher and the lower energy sides relative to the bulk. This is because of the disturbed atomic arrangement at the grain boundary. When the defects are introduced, acceptor-type levels form mainly by the oxygen ions adjacent to the vacancy or at the interstitial site, as is the case of the bulk models. For both of the defects, the energies are slightly higher than the top of the valence band of the boundary model without the defects. The formation of acceptor-type levels is similar to the case of oxygen–atom- or oxygen–molecule-adsorbed surfaces.[32,64]

The energies of the highest occupied levels are listed with the formation energies in Table IV. The values for the oxygen interstitial at the bulk tetrahedral site and the zinc vacancy at the boundary A site are also shown. By the presence of the defects, the energies of the highest occupied levels are increased, as also recognized in Fig. 4. In the bulk, the increase by the zinc vacancy is 0.2 eV. The oxygen interstitials, which have higher formation energies than the vacancy, generate the higher energy levels of 1.3 and 1.4 eV relative to the bulk valence band edge. At the grain boundary, the formation energies are lower than those in the bulk for both the zinc vacancy and the oxygen interstitial. For the zinc vacancy at the C site, which has the lowest formation energy among all the defects dealt in the present study, the increase of the highest level energy is 0.2 eV relative to the original configuration without the defects. This value is the same as the vacancy in the bulk. On the other hand, the increase of 0.5 eV by the interstitial oxygen is considerably smaller than those in the bulk. The one-electron energy levels associated with the defects seem to be related to the formation energies by the static lattice calculation.

Chemical bonding around the defects is discussed using the results of Mulliken population analysis. They are summarized in Table V. For the defect models, the averaged values of the oxygen ions adjacent to the va-

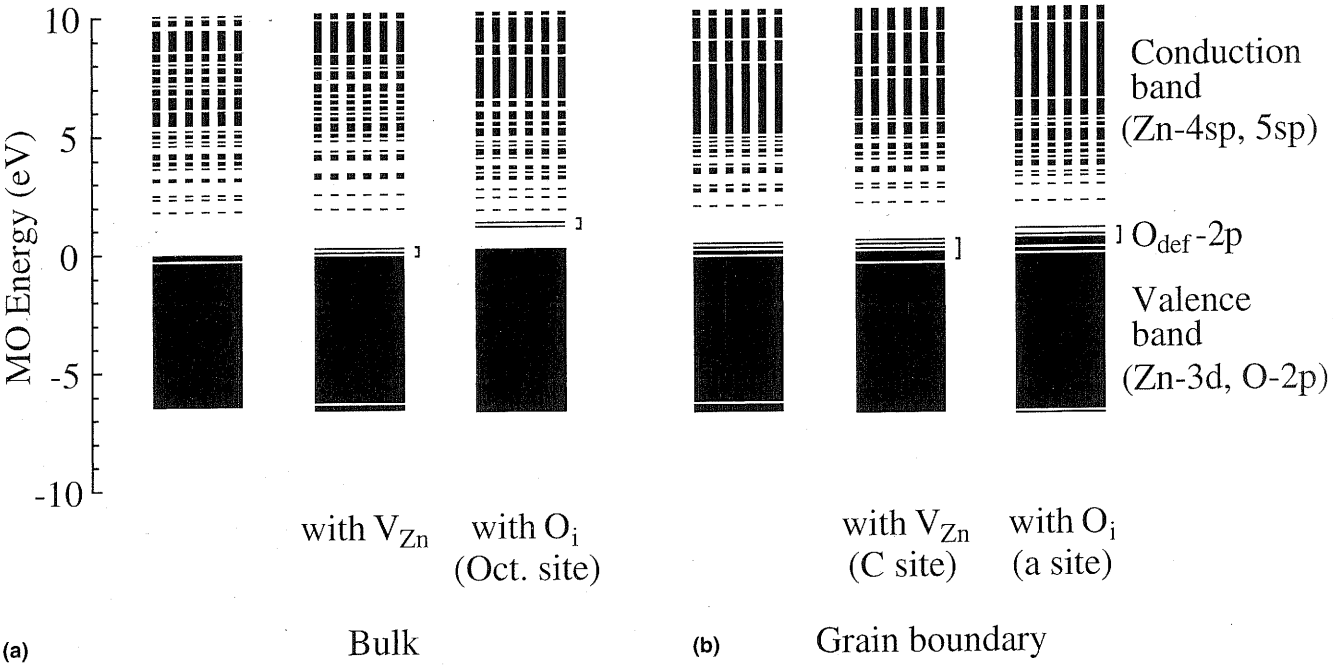

FIG. 4. Energy level diagrams for (a) the bulk and (b) the grain boundary model clusters. Solid and broken bars denote occupied and unoccupied levels. The distribution of the 2p components by the oxygen ions adjacent to the vacancies or at the interstitial sites is marked as O_{def} – 2p.

TABLE IV. Energies of the highest occupied levels and the defect formation. The energy of the highest occupied level is relative to that of the bulk model without the defects. For the grain boundary models, the differences from the grain boundary model without the defects are also shown in the parentheses.

	Defect	Energy of the highest occupied level	Formation energy (eV)
Bulk	V_{Zn}	0.2	3.7
	O_i (Octahedral site)	1.3	4.6
	O_i (Tetrahedral site)	1.4	6.3
Grain boundary	No	0.3	···
	V_{Zn} (A site)	0.7 (0.4)	2.8
	V_{Zn} (C site)	0.5 (0.2)	2.4
	O_i (a site)	0.8 (0.5)	3.4

TABLE V. Net charge and overlap population with respect to oxygen ions. For the defect models, the net charge is the averaged value of the oxygen ions adjacent to the vacancy or the value of the oxygen interstitial, and the averaged value of their neighboring zinc ions. The overlap population is the averaged value with respect to the oxygen ions. Plus and minus values denote bonding and antibonding interactions, respectively. For the O–Zn component, the coordination numbers are shown in the parentheses.

		Net charge		Overlap population		
	Defect	O	Zn	O–Zn	Others	Total
Bulk	No	−1.09	1.08	0.95(4)	−0.14	0.81
	V_{Zn}	−1.14	1.13	0.90(3)	−0.15	0.75
	O_i (Octahedral site)	−1.09	1.10	0.91(6)	−0.65	0.26
Grain boundary	No	−1.10	1.09	0.87(4)	−0.13	0.74
	V_{Zn} (C site)	−1.18	1.16	0.87(3)	−0.18	0.69
	O_i (a site)	−1.06	1.11	0.88(4)	−0.27	0.61

cancies or the value of the oxygen interstitials, and the overaged values of their neighboring zinc ions are shown.

For the bulk model without the defects, zinc and oxygen ions have the net charges of about ±1.1, respectively. When a zinc vacancy in the charge state 2– is introduced, two extra electrons should be shared by the ions around the vacancy. If the oxygen ions adjacent to the vacancy share all of the charge, this should correspond to the change of the net charge by –0.5 per oxygen ion from the bulk value. In practice, the electrons distribute more widely, and therefore, the change of the net charge is very small. Regarding the overlap population, major contribution is given by the bonding interaction with neighboring zinc ions. Others consist mainly of the antibonding interaction with the neighboring oxygen ions. The presence of the vacancy in the bulk affects the overlap population slightly. For the O–Zn component, although the coordination number is reduced to 3, each of the three bonding interactions is reinforced to make the sum close to the value of the perfect lattice. For the oxygen interstitial, it is interesting that the charge is almost the same as those of oxygen ions in the bulk without the defects. However, the total overlap population is considerably reduced. This is mainly due to the antibonding interaction with closely surrounding oxygen ions, which is included in the component "Others." The unfavorable surroundings as discussed in Sec. II. B should result in the considerable weakness of the covalent bonding.

For the grain boundary without the defects, the averages of the net charges of the oxygen and zinc ions adjacent to the fourfold and eightfold coordinated channels and the average of overlap populations with respect to the oxygen ions are shown. The chemical bonding state is very close to that in the bulk without the defects: only the slight decrease in the overlap population is recognized. The features of the change in chemical bonding brought by the defects are also similar to the case of the bulk, except that the reduction of the overlap population by the presence of the oxygen interstitial is suppressed. This is mainly due to the smaller antibonding interactions with neighboring oxygen ions at the larger distance than the case of the bulk oxygen interstitial, as mentioned in Sec. II. B. Thus the disturbance of chemical bonding states by the defects is smaller at the grain boundary, especially for the oxygen interstitial. This is consistent with the lower formation energies obtained by the static lattice calculation.

In ZnO varistors, interfacial electronic states have been detected experimentally at 0.6–1.0 eV below the bottom of the conduction band by the methods such as the deep-level transient spectroscopy (DLTS) and the isothermal transient spectroscopy.[8–13] This corresponds to 2.3–2.7 eV above the top of the valence band according to the experimental band gap of 3.30 eV.[63] The electronic states are unoccupied since only unoccupied states are detectable by the methods. Occupied states are expected to exist at the lower energy side.[18,19] In the present study, the electronic states associated with the zinc vacancy at the C site, which has the lowest formation energy among the present defects, form at 0.5 above to the top of the valence band of the bulk model. The states are occupied due to the assumption of the charge state of 2–, which corresponds to the trapping of two electrons. Because the energies of the states are very low, they are likely to have the charge state under the high Fermi energies of varistors.[13] Although the calculations are done only for a limited number of geometries, the present results imply that the point defects associated with the oxygen excess at the grain boundary most likely induce occupied defect states close to the top of the valence band in general. Because there seems to be a correlation between the one-electron energies of the defect levels and the formation energies, the presence of much higher defect levels, which may be induced by the defects with much higher formation energies, is unlikely even at boundaries with arbitrary orientations. The defect states are expected to work to trap electrons as assumed in the present study and to generate the double Schottky barrier. On the other hand, impurities should play central roles for higher interface states as experimentally detected. They may be electronic states specific to the impurities such as d states of 3d transition elements. Other possible origin is intrinsic defects with high formation energies, like the bulk oxygen interstitial in the present study: the association with the impurities may facilitate the formation of the defects, and this may induce high energy states in the boundary region.

IV. SUMMARY

Zinc vacancies and oxygen interstitials at the ZnO [0001]/($1\bar{2}30$) symmetric tilt boundary have been investigated by the combination of static lattice and first-principles molecular orbital methods. For both of the zinc vacancies and the oxygen interstitials, the formation energies are lower than those of the bulk defects at certain sites in the grain boundary. Regarding the electronic structure, energy levels specific to the defects form near the top of the valence band. At the grain boundary, the energies of the defect levels relative to the valence levels of the configuration without the defects are lower than those in the bulk. The disturbance of chemical bonding states by the defects is also smaller, especially for the oxygen interstitial. This tendency is consistent with the formation energies obtained by the static lattice calculations. Although the calculations are performed only for limited number of geometries, the present results imply that the point defects associated with the oxygen excess at the grain boundary most likely induce defect states

close to the top of the valence band in general. For higher interface states as experimentally detected, the effects of impurities should be significant.

ACKNOWLEDGMENTS

We are grateful to Julian D. Gale for allowing us to use the computer code GULP and Ben Slater and David H. Gay for their support and helpful discussions. This study was performed through Special Coordination Funds of the Science and Technology Agency (STA) and the ACT program of Japan Science and Technology Corporation (JST).

REFERENCES

1. D.R. Clarke, J. Am. Ceram. Soc. **82,** 485 (1999).
2. M. Matsuoka, Jpn. J. Appl. Phys. **10,** 736 (1971).
3. K. Mukae, K. Tsuda, and I. Nagasawa, Jpn. J. Appl. Phys. **16,** 1361 (1977).
4. G.E. Pike and C.H. Seager, J. Appl. Phys. **50,** 3414 (1979).
5. G.E. Pike, S.R. Kurtz, P.L. Gourley, H.R. Philipp, and L.M. Levinson, J. Appl. Phys. **57,** 5512 (1985).
6. G. Blatter and F. Greuter, Phys. Rev. B **34,** 8555 (1986).
7. K. Mukae, Key Eng. Mater. **125/126,** 317 (1997).
8. J.P. Gambino, W.D. Kingery, G.E. Pike, H.R. Philipp, and L.M. Levinson, J. Appl. Phys. **61,** 2571 (1987).
9. K. Tsuda and K. Mukae, J. Ceram. Soc. Jpn. **97,** 1211 (1989).
10. M. Hayashi, M. Kuramoto and M. Hayashi, in *Advances in Varistor Technology,* edited by L.M. Levinson (American Ceramic Society, Westerville, OH, 1989), p. 364.
11. T. Maeda, S. Meguro, and M. Takata, Jpn. J. Appl. Phys. **28,** L714 (1989).
12. R.A. Winston and J.F. Cordaro, J. Appl. Phys **68,** 6495 (1990).
13. K. Tsuda and K. Mukae, J. Ceram. Soc. Jpn. **100,** 1239 (1992).
14. F. Oba, I. Tanaka, S.R. Nishitani, H. Adachi, B. Slater, and D.H. Gay, Philos. Mag. A **80,** 1567 (2000).
15. D.G. Brandon, B. Ralph, S. Ranganathan, and M.S. Wald, Acta Metall. **12,** 813 (1964).
16. S.D. Mo, W.Y. Ching, and R.H. French, J. Am. Ceram. Soc. **79,** 627 (1996).
17. I. Dawson, P.D. Bristowe, M.H. Lee, M.C. Payne, M.D. Segall, and J.A. White, Phys. Rev. B **54,** 13727 (1996).
18. F. Greuter, G. Blatter, M. Rossinelli, and F. Schmückle, Mater. Sci. Forum **10–12,** 235 (1986).
19. F. Greuter, G. Blatter, M. Rossinelli, and F. Stucki, in *Advances in Varistor Technology,* edited by L.M. Levinson (American Ceramic Society, Westerville, OH, 1989), p. 31.
20. E. Sonder, M.M. Austin, and D.L. Kinser, J. Appl. Phys. **54,** 3566 (1983).
21. S. Fujitsu, H. Toyoda, and H. Yanagida, J. Am. Ceram. Soc. **70,** C71 (1987).
22. F. Stucki, P. Brüesch, and F. Greuter, Surf. Sci. **189/190,** 294 (1987).
23. F. Stucki and F. Greuter, Appl. Phys. Lett. **57,** 446 (1990).
24. F.A. Kröger, *The Chemistry of Imperfect Crystals* (North-Holland, Amsterdam, The Netherlands, 1974), Vol. 2, p. 743.
25. K.I. Hagemark and L.C. Chacka, J. Solid State Chem. **15,** 261 (1975).
26. M.H. Sukkar and H.L. Tuller, in *Advances in Ceramics,* edited by M.F. Yan and A.H. Heuer (American Ceramic Society, Columbus, OH, 1983), Vol. 7, p. 71.
27. J.C. Simpson and J.F. Cordaro, J. Appl. Phys. **67,** 6760 (1990).
28. Y. Yano, Y. Shirakawa, and H. Morooka, Jpn. J. Appl. Phys. **31,** L1429 (1992).
29. Y. Yano, Y. Takai, and H. Morooka, J. Mater. Res. **9,** 112 (1994).
30. S. Fujitsu, K. Koumoto, and H. Yanagida, Solid State Ionics **32/33,** 482 (1989).
31. M. Yodogawa, Y. Ikuhara, F. Oba, and I. Tanaka, Key Eng. Mater. **157–158,** 24 (1999).
32. F. Oba, I. Tanaka, and H. Adachi, Jpn. J. Appl. Phys. **38,** 3569 (1999).
33. K.L. Merkle and D.J. Smith, Phys. Rev. Lett. **59,** 2887 (1987).
34. K.L. Merkle, J.F. Reddy, C.L. Wiley, and D.J. Smith, J. Phys. **49,** C5–251 (1988).
35. T. Höche, P.R. Kenway, H.-J. Kleebe, M. Rühle, and P.A. Morris, J. Am. Ceram. Soc. **77,** 339 (1994).
36. A.N. Kiselev, F. Sarrazit, E.A. Stepantsov, E. Olsson, T. Claeson, V.I. Bondarenko, R.C. Pond, and N.A. Kiselev, Philos Mag. A **76,** 633 (1997).
37. D.M. Duffy and P.W. Tasker, Philos. Mag. A. **47,** 817 (1983).
38. D.M. Duffy and P.W. Tasker, Philos. Mag. A. **48,** 155 (1983).
39. P.W. Tasker and D.M. Duffy, Philos. Mag. A. **47,** L45 (1983).
40. M. Meyer and C. Waldburger, Mater. Sci. Forum **126–128,** 229 (1993).
41. P.R. Kenway, J. Am. Ceram. Soc. **77,** 349 (1994).
42. A.P. Sutton and R.W. Balluffi, *Interfaces in Crystalline Materials* (Oxford University Press, New York, 1995), p. 318.
43. W. Wunderlich, Phys. Stat. Solidi (a) **170,** 99 (1998).
44. J.D. Gale, J. Chem. Soc., Faraday Trans. **93,** 629 (1997).
45. W.H. Press, S.A. Teukolsky, W.T. Vetterling and B.P. Flannery, *Numerical Recipes,* 2nd ed. (Cambridge University Press, Cambridge, United Kingdom, 1992), p. 418.
46. G.V. Lewis and C.R.A. Catlow, J. Phys. C: Solid State Phys. **18,** 1149 (1985).
47. S.C. Abrahams and J.L. Bernstein, Acta Crystallogr., Sect. B **25,** 1233 (1969).
48. T.B. Bateman, J. Appl. Phys. **33,** 3309 (1962).
49. H. Karzel, W. Potzel, M. Köfferlein, W. Schiessl, M. Steiner, U. Hiller, G.M. Kalvius, D.W. Mitchell, T.P. Das, P. Blaha, K. Schwarz, and M.P. Pasternak, Phys. Rev. B **53,** 11425 (1996).
50. N.F. Mott and M.J. Littleton, Trans. Faraday Soc. **34,** 485 (1938).
51. C.R.A. Catlow, R. James, W.C. Mackrodt, and R.F. Stewart, Phys. Rev. B **25,** 1006 (1982).
52. A. Rohatgi, S.K. Pang, T.K. Gupta, and W.D. Straub, J. Appl. Phys. **63,** 5375 (1988).
53. G.A. Baraff and M. Schlüter, Phys. Rev. Lett. **55,** 1327 (1985).
54. Jörg Neugebauer and C.G. Van de Walle, Phys. Rev. B **50,** 8067 (1994).
55. W. Orellana and H. Chacham, Appl. Phys. Lett. **74,** 2984 (1999).
56. M.C. Payne, M.P. Teter, D.C. Allan, T.A. Arias, and J.D. Joannopoulos, Rev. Mod. Phys. **64,** 1045 (1992).
57. D.B. Laks, C.G. Van de Walle, G.F. Neumark, P.E. Blöchl, and S.T. Pantelides, Phys. Rev. B **45,** 10965 (1992).
58. D.E. Ellis, H. Adachi, and F.W. Averill, Surf. Sci. **58,** 497 (1976).
59. H. Adachi, M. Tsukada, and C. Satoko, J. Phys. Soc. Jpn. **45,** 875 (1978).
60. R.S. Mulliken, J. Chem. Phys. **23,** 1833 (1955).
61. P. Schröer, P. Krüger, and J. Pollmann, Phys. Rev. B **47,** 6971 (1993).
62. Y.N. Xu and W.Y. Ching, Phys. Rev. B **48,** 4335 (1993).
63. V. Srikant and D.R. Clarke, J. Appl. Phys. **83,** 5447 (1998).
64. M.H. Sukkar, K.H. Johnson, and H.L. Tuller, Mater. Sci. Eng. B **6,** 49 (1990).